Title:
A METHOD TO ESTIMATE CLIMATE-CRITICAL CONSTRUCTION MATERIALS APPLIED TO SEAPORT PROTECTION

Authors:
Austin Becker ◇, Nathan Chase⁘, Martin Fischer ⁘, Ben Schwegler ◆, Keith Mosher ☆

Author affiliations:
◇ Department of Marine Affairs, University of Rhode Island, Coastal Institute Room 213, 1 Greenhouse Road, Suite 205, Kingston, RI 02881
⁘ Nathan Chase, PE– RMC Water and Environment
◆ Ben Schwegler, PhD, Civil and Environmental Engineering, Stanford University
⁘ Martin Fischer, PhD, – Civil and Environmental Engineering, Stanford University
☆ Keith Mosher, MS– Mosher Consulting/Stanford University

Corresponding author:
Austin Becker, PhD
Department of Marine Affairs
University of Rhode Island, Coastal Institute Room 213, 1 Greenhouse Road, Suite 205, Kingston, RI 02881
e: abecker@uri.edu | p: 401-874-4192 | f: 401-874-2156

Cite as:
Becker, A., Chase, N.T.L., Fischer, M., Schwegler, B., Mosher, K. (2016) A method to estimate climate-critical construction materials applied to seaport protection. Global Environmental Change, 40, 125-136,DOI 10.1016/j.gloenvcha.2016.07.008, ISSN 09593780.

Appendix A. – Selection of Ports

It would not be feasible to generate estimates for all 3,300+ seaports in the world with a reasonable effort; thus, selecting a sample of seaports requires limiting criteria (e.g., by economic criteria, social/environmental justice, political significance, military strength). In this case, we selected the world's most important seaports by economic value and population served. We included the top 100 coastal seaports by tonnage volume (AAPA 2011; NGIA 2014) and all coastal seaports identified in the World Port Index that were located within or nearby a metropolitan area with a population of approximately one million or more, as projected for 2015 (Nordpil, 2009). This resulted in 221 seaports (Figure A1 and Table A1).

Figure A1 -- Map of 221 seaports in project study

Table A1 -- Table of 221 seaports included in study (ports included had *either* population over 1m *or* were in the top 100f or throughput in 2013 or both)

City Name	Port Name	Country	Region
Abidjan	Abidjan	Côte d'Ivoire	Africa
Alexandria	Alexandria	Egypt	Africa
Benghazi	Benghazi	Libya	Africa
Cape Town	Cape Town	South Africa	Africa
Conakry	Conakry	Guinea	Africa
Dakar	Dakar	Senegal	Africa
Dar-el-Beida	Casablanca	Morocco	Africa
Dar-es-Salaam	Dar-es-Salaam	Tanzania	Africa
Douala	Douala	Cameroon	Africa
Durban	Durban	South Africa	Africa
El Djazir	Skikkda (Algier)	Algeria	Africa
Lagos	Lagos	Nigeria	Africa
Lom	Lom	Togo	Africa

Luanda	Luanda	Angola	Africa
Maputo	Maputo	Mozambique	Africa
Monrovia	Monrovia	Liberia	Africa
Muqdisho	Muqdisho	Somalia	Africa
Port Elizabeth	Port Elizabeth	South Africa	Africa
Richards Bay	Richards Bay	South Africa	Africa
Said Port (East)	Said Port (East)	Egypt	Africa
Saldanha Bay	Saldanha Bay	South Africa	Africa
Tanger	Tanger	Morocco	Africa
Tema	Tema	Ghana	Africa
Tripoli	Tripoli	Libya	Africa
Ban Hlem Chabang	Laem Chabang	Thailand	Asia
Bangkok	Bangkok	Thailand	Asia
Busan	Busan	South Korea	Asia
Chennai	Madras (Chennai)	India	Asia
Chittagong	Chittagong	Bangladesh	Asia
Colombo	Colombo	Sri Lanka	Asia
Constantza	Romania	Russia	Asia
Daesan	Daesan	South Korea	Asia
Dalian	Dalian	China	Asia
Dhaka	Dhaka	Bangladesh	Asia
Fuzhou Fujian	Fuzhou Fujian	China	Asia
Guangzhou	Guangzhou	China	Asia
Hai Phong	Hai Phong	Vietnam	Asia
Hangzhou	Hangzhou	China	Asia
Hiroshima	Hiroshima	Japan	Asia
Ho Chi Minh	Saigon (Saigon New Port)	Vietnam	Asia
Hong Kong	Hong Kong	China	Asia
Inchon	Inchon	South Korea	Asia
Jawaharlal Nehru	Jawaharlal Nehru	India	Asia
Kaohsiung	Kaohsiung	Taiwan	Asia
Karachi	Karachi	Pakistan	Asia
Keelung	Keelung	Taiwan	Asia
Kelang	Kelang	Malaysia	Asia
Khulna	Khulna	Bangladesh	Asia
Kitakyushu	Kitakyushu	Japan	Asia
Kobe	Kobe	Japan	Asia
Kochi	Kochi	India	Asia
Kolkata	Kolkata	India	Asia
Kota Baru	Kota Baru	Indonesia	Asia
Kwangyang	Kwangyang	South Korea	Asia

Manila	Manila	Philippines	Asia
Mormugao	Mormugao	India	Asia
N'ampo	N'ampo	North Korea	Asia
Nagoya	Nagoya	Japan	Asia
Ningbo	Ningbo	China	Asia
Paradip	Paradip	India	Asia
Penang	Penang	Malaysia	Asia
Pohang	Pohang	South Korea	Asia
Qingdao	Qingdao	China	Asia
Qinhuangdao	Qinhuangdao	China	Asia
Quanzhou	Quanzhou	China	Asia
Rangoon	Rangoon	Myanmar	Asia
Sapporo	Sapporo	Japan	Asia
Semarang	Semarang	Indonesia	Asia
Sendai	Sendai	Japan	Asia
Shanghai	Shanghai	China	Asia
Shantou	Shantou	China	Asia
Singapore	Singapore	Singapore	Asia
Surat	Surat	India	Asia
Taichung	Taichung	Taiwan	Asia
Tanjung Priok (Jakarta)	Tanjung Priok (Jakarta)	Indonesia	Asia
Tianjin	Tianjin	China	Asia
Ulsan	Ulsan	South Korea	Asia
Visakhapatnam	Visakhapatnam	India	Asia
Wenzhou	Wenzhou	China	Asia
Xiamen	Xiamen	China	Asia
Yantai	Yantai	China	Asia
Yokohama	Yokohama	Japan	Asia
Zhanjiang	Zhanjiang	China	Asia
Zhuhai	Zhuhai	China	Asia
Algeciras	Algeciras	Spain	Europe
Amsterdam	Amsterdam	Netherlands	Europe
Athens	Paraeus	Greece	Europe
Barcelona	Barcelona	Spain	Europe
Bremen	Bremen	Germany	Europe
Bremerhaven	Bremerhaven	Germany	Europe
Copenhagen	Copenhagen	Denmark	Europe
Dublin	Dublin	Ireland	Europe
Dunkirk	Dunkirk	France	Europe
Felixstowe	Felixstowe	United Kingdom	Europe
Genoa	Genoa	Italy	Europe
Gioia Tauro	Gioia Tauro	Italy	Europe

Glasgow	Clyde	United Kingdom	Europe
Gothenburg	Gothenburg	Sweden	Europe
Grimsby and Immingham	Grimsby and Immingham	United Kingdom	Europe
Hamburg	Hamburg	Germany	Europe
Helsinki	Helsinki	Finland	Europe
La Spezia	La Spezia	Italy	Europe
Las Palamas	Las Palamas	Spain	Europe
Le Havre	Le Havre	France	Europe
Leixoes	Leixoes	Portugal	Europe
Lisbon	Lisbon	Portugal	Europe
London	London	United Kingdom	Europe
Malmo	Malmo	Sweden	Europe
Marseilles	Marseilles	France	Europe
Milford Haven	Milford Haven	United Kingdom	Europe
Napoli	Napoli	Italy	Europe
Novorossiysk	Novorossiysk	Russia	Europe
Odessa	Odessa	Ukraine	Europe
Primorsk	Primorsk (Baltic Sea)	Russia	Europe
Rotterdam	Rotterdam	Netherlands	Europe
Southampton	Southampton	United Kingdom	Europe
St. Petersburg	St. Petersburg	Russia	Europe
Stockholm	Stockholm	Sweden	Europe
Treiste	Treiste	Italy	Europe
Valencia	Valencia	Spain	Europe
Zeebrugge	Zeebrugge	Belgium	Europe
Ambarli	Ambarli	Turkey	Middle East
Ashdod	Ashdod	Isreal	Middle East
Bandar Abbas	Bandar Abbas	Iran	Middle East
Beirut	Beirut	Lebanon	Middle East
Dammam	Dammam	Saudi Arabia	Middle East
Dubai	Dubai	United Arab Emirates	Middle East
Heifa	Heifa	Isreal	Middle East
Icel (Mersin)	Icel (Mersin)	Turkey	Middle East
Istanbul	Istanbul	Turkey	Middle East
Izmir	Izmir	Turkey	Middle East
Izmit (Kocaeli)	Izmit (Kocaeli)	Turkey	Middle East
Jeddah	Jeddah	Saudi Arabia	Middle East
Jubail	Jubail	Saudi Arabia	Middle East
Khawr Fakkan	Khawr Fakkan	United Arab Emirates	Middle East
Kuwait City	Shaiba and Shuwaikh	Kuwait	Middle East

Salalah	Salalah	Oman	Middle East
Anchorage	Anchorage	U.S.	North America
Baltimore	Baltimore	U.S.	North America
Beaumont(TX)	Beaumont(TX)	U.S.	North America
Boston	Boston	U.S.	North America
Canaveral	Canaveral	U.S.	North America
Charleston	Charleston	U.S.	North America
Corpus Christi	Corpus Christi	U.S.	North America
Freeport	Freeport	Bahamas	North America
Galveston	Galveston	U.S.	North America
Gulfport	Gulfport	U.S.	North America
Halifax	Halifax	Canada	North America
Havana	Havana	Cuba	North America
Honolulu	Honolulu	U.S.	North America
Houston	Houston	U.S.	North America
Hueneme	Hueneme	U.S.	North America
Jacksonville	Jacksonville	U.S.	North America
Kahului	Kahului	U.S.	North America
Kingston	Kingston	Jamaica	North America
Lake Charles	Lake Charles	U.S.	North America
Long Beach	Long Beach	U.S.	North America
Manzillo (Mexico)	Manzillo (Mexico)	Mexico	North America
Manzillo (Panama)	Manzillo (Panama)	Panama	North America

Miami	Miami	U.S.	North America
Mobile	Mobile	U.S.	North America
New Orleans	New Orleans	U.S.	North America
New York/New Jersey	New York/New Jersey	U.S.	North America
Oakland	Oakland	U.S.	North America
Philadelphia	Philadelphia	U.S.	North America
Port-au-Prince	Port-au-Prince	Haiti	North America
Portland	Portland	U.S.	North America
Providence	Providence	U.S.	North America
Redwood City	Redwood City	U.S.	North America
Saint John	Saint John	Canada	North America
San Diego	San Diego	U.S.	North America
San Francisco	San Francisco	U.S.	North America
San Juan(PR)	San Juan(PR)	U.S.	North America
Santo Domingo	Santo Domingo	Dominican Republic	North America
Savannah	Savannah	U.S.	North America
Seattle	Seattle	U.S.	North America
St. John's	St. John's	Canada	North America
Tampa-St. Petersburg	Tampa-St. Petersburg	U.S.	North America
Vancouver	Vancouver	Canada	North America
Virginia Beach	Virginia Beach	U.S.	North America
Washington D.C.	Washington D.C.	U.S.	North America
Wilmington(NC)	Wilmington(NC)	U.S.	North America

Adelaide	Adelaide	Australia	Oceania
Auckland	Auckland	New Zealand	Oceania
Brisbane	Brisbane	Australia	Oceania
Dampier	Dampier	Australia	Oceania
Davao	Davao	Philippines	Oceania
Gladstone	Gladstone	Australia	Oceania
Hay Point	Hay Point	Australia	Oceania
Melbourne	Melbourne	Australia	Oceania
Newcastle	Newcastle	Australia	Oceania
Palembang	Palembang	Indonesia	Oceania
Perth	Fremantle	Australia	Oceania
Port Hedland	Port Hedland	Australia	Oceania
Surabaya	Surabaya	Indonesia	Oceania
Sydney	Sydney	Australia	Oceania
Angra dos Reis	Angra dos Reis	Brazil	South America
Barranquilla	Barranquilla	Colombia	South America
Belem	Belem	Brazil	South America
Buenos Aires	Buenos Aires	Argentina	South America
Caracas	Caracas	Venezuela	South America
Cartagena	Cartagena	Colombia	South America
Fortaleza	Fortaleza	Brazil	South America
Grande Vitoria	Grande Vitoria	Brazil	South America
Guayaquil	Guayaquil	Ecuador	South America
Itajai/Navagantes	Itajai/Navagantes	Brazil	South America
Itaqui	Itaqui	Brazil	South America
Lima	Lima	Peru	South America
Maceio	Maceio	Brazil	South America
Maracaibo	Maracaibo	Venezuela	South America
Montevideo	Montevideo	Uruguay	South America
Natal	Natal	Brazil	South

			America
			South
Panama City	Panama City	Panama	America
			South
Paranagua	Paranagua	Brazil	America
			South
Porto Alegre	Porto Alegre	Brazil	America
			South
Recife	Recife	Brazil	America
			South
Salvador	Salvador	Brazil	America
			South
Santos	Santos	Brazil	America
			South
Sao Sebastiao	Sao Sebastiao	Brazil	America
			South
Sepetiba	Sepetiba	Brazil	America
			South
Tubarao	Tubarao	Brazil	America

Appendix B – The elevation/topography data and algorithm used to create the model paths

Our model operated by creating a graph of weighted nodes for each elevation or bathymetry data point, and then comparing the required materials of all possible paths surrounding the port infrastructure. The path consideration and choice utilized Dykstra's algorithm (Dijkstra, 1959). Because the weighting of our "model path" was based on minimizing materials, the path itself could be quite long as it snaked around the port looking for the highest available elevation points in order to minimize the amount of new structure required. On inspection, it demonstrated a sophisticated use of natural terrain to avoid building structures where natural features already provided protection.

Our "model path" also depended on the extent of elevation data that the model was allowed to run over. We could manually adjust the extent, covering more territory east/west or north/south. However, the larger the extent, the longer the computation would take. To ensure optimal 'correct' modeling, we increased the grid size for each port and re-ran the model until the material volume and path reached a steady state and stopped changing for grid size changes. We selected the smallest simulation grid from the steady state for future simulations. This captured the local usable terrain features and optimized the modeling time. Changing the model extent around each port had either no effect (e.g., when the port was at the base of a hill) or a very large effect (e.g., when the port was in an emergent coastal area with a very gradual slope) depending on whether a longer but more efficient path was available. In some cases, two ports are in such proximity to each other that a single protection system was created for both ports. These multi-port structures include the ports of Seattle and Tacoma; Kobe and Osaka; Singapore and Tanjung Pelepas; and Hong Kong and Shenzhen. The port protector model is intended to provide approximations to develop aggregate estimates of materials requirements and to understand risks in very large systems, so high precision is not as valuable as dependable and repeatable order-of-magnitude values that can include many subjects (in this case, ports).

The model identifies all of the possible paths for enclosing and protecting the designated port structures to the target elevation using a combination of three design structures and the existing topography. The material required to construct each path option is compared, and the lowest materials path is chosen. The higher the resolution of the bathymetry and elevation data, the more accurate the model path will be, as the model path simply connects the dots between datapoints in order to generate an average structure depth and height. However, the lack of availability of a global set of high-resolution elevation data, as well as the increased simulation time to run the model, made a lower-resolution dataset a more practical alternative. Shuttle Radar Topography Mission (SRTM) data, publicly available through Google Earth has 30 arc-second resolution and is available on a global scale (USGS2004). Land elevations were collected in February 2000 by a radar system on

the Space Shuttle Endeavor and combined with ocean soundings from the Smith and Sandwell 1-minute grid and various higher definition bathymetry projects. Thus, we chose SRTM as our starting point, as it is available to everyone and covers all of the populated areas of the globe with comparable quality and resolution data.

However, since resolution of elevation data and grid size of data could affect the model outputs, we examined the sensitivity of the model to two different resolutions of data. A lower density grid of elevation points (i.e., lower resolution data) would ostensibly cover the same distance, but could miss structural considerations like channels or shoals, and might force the structure to be 'built' on a sub-optimal path. Deep navigation channels, for example, could cause an underreporting of materials required (the actual structure required would be deeper than estimated if two bathymetric datapoints fell on either side of the channel) and shoals could cause an over-reporting (estimating a deeper structure than required).

We thus conducted a sensitivity analysis using the highest resolution data we could find for a sample of ports. We selected 10 ports around the US and used NOAA electronic charts for bathymetry and LIDAR elevation data for elevation. This required us to “stitch together” the two datasets using ARCGIS extracting a new grid of elevation points. The resulting data was integrated and rasterized, extracting an elevation data grid with a 30 meter (1 arc second) resolution for the following 10 US ports, chosen to represent a cross-section of geomorphological characteristics around the US:

- Gulfport, MS
- Tampa, FL
- San Diego, CA
- Oakland, CA
- Miami, FL
- Long Beach, CA
- Charleston, SC
- Corpus Christi, TX
- Boston, MA
- Baltimore, MD

The 10 test ports were run with both 30-arc second (SRTM) and 1-arc second (using NOAA e-charts and LIDAR) datasets to test the results from the two different resolutions of data (Table B1).

Table B1 - Comparison of model runs using low resolution vs. high resolution data

Port Name	Materials required (millions of m^3) (low resolution data)	Materials required (millions of m^3) (high resolution data)	Ratio of low resolution to high resolution
San Diego	2.2	2.2	1.0
Boston	1.9	2.0	0.9
Baltimore	2.3	2.0	1.1
Long Beach	12.0	10.4	1.2
Tampa-St. Petersburg	3.8	3.2	1.2
Gulfport	2.3	1.7	1.4
Miami	1.4	0.9	1.5
Charleston	4.4	2.1	2.1
Corpus Christi	2.3	0.7	3.3
Oakland	3.0	0.9	3.3
Average	**3.6**	**2.6**	1.4

Of the 10 ports, eight produced model runs that used less material volume when using the higher resolution data, which lines up with expectations. On average, the low-resolution data produced results with about 1.4 times *more* materials than the model run using the high-resolution data. The modeling time was seconds per port with the low resolution elevation grid, and over an hour per port for the high resolution model runs.

Given the broad strokes and imprecision in output values inherent in a MACD, and the high cost and difficulty of obtaining higher precision elevation data (not to mention longer simulation times and costs), we deem the SRTM data and the 30-arc second elevation data credible for the desired output accuracy. Furthermore, use of the SRTM data allows easier replication and transfer to other problems under consideration for similar modeling.

Appendix C – Calculating materials using the Port Protector

The application of the MACD approach resulted in both a design and a spreadsheet that considers the 3-segment design and its component parts shown in the main

paper and also in Figures D1-D3. The spreadsheet considered the choice and materials requirements for each of the three structures over their anticipated applicable height range. Looking at the current elevation land adjacent to a port and comparing that elevation with the required height to protect against the projected future sea level gave a target structure height, and the different components of the design scaled separately to meet the target height. The spreadsheet calculations were extracted and implemented in Python code, which formed the heart of the simulation model. All told, the spreadsheet produced almost 200 interconnected equations to generate the segment materials profiles.

The simulation program takes as inputs a latitude/longitude grid of elevation points surrounding a port, a polygon defined in latitude and longitude that covers the port infrastructure (manually created from satellite maps), and manually chosen start and end polygons that bracket the port, a value for height of sea level rise (SLR), which can be changed from simulation to simulation to compare scenarios. For this run, we used tidal data for the port in the form of the mean high high-water (MHHW), a projected 1000-year storm surge height for the port, and an engineering safety multiplication factor of 1.1 applied to the storm surge variable to result in a structure height that can effectively deal with a 2 meter SLR and the projected surge.

Estimating the return period for storm surge for specific ports in different countries and regions proved to be outside the scope of this study (Muis et al., 2016). Thus, we relied on the DIVA database (Hinkel et al., 2012; Vafeidis et al., 2008) to derive a rough calculation of expected surge heights to determine DWSEL for the structures in each port. When we began the study, the DIVA database was publically available for download, thus our calculations are based on the version accessed in 2011. Although this database does not include information about the ports themselves, it provides a rich set of information for each port city, including a calculation for projected storm surge at 1 in 1, 1 in 10, 1 in 100, and 1 in 1000-year surge height (in base year) above mean high water. We used the 1 in 1000-year surge height to calculate DWSEL for our model run. Of the 221 ports included in our study, 180 of the cities adjacent to or encompassing these ports were also included in the DIVA database. For the 41 ports that were not included in DIVA, we did not have an accurate surge height probability available. Since calculating projected surge heights was beyond the scope of this study, we elected to use the mean surge calculation for the nearest port or ports in the DIVA database that roughly shared the geomorphological characteristics of the port in question (e.g., same coastline, at a river mouth, protected or not projected by a headland). The tidal data and the surge data obtained from the DIVA database and were not further modified except for interpolation of both surge and tidal values for ports not evaluated in that project.

The simulation starts with the calculation for a port in a scenario of the Design Water Surface Elevation (DWSEL), which is the elevation required for all of the protective structure to reach. DWSEL = MHHW + SLR + (1000-year Storm Surge * 1.1).

The simulation next takes the elevation grid and compares and records the average elevation of each adjacent pair of elevation points (a segment). These elevations represent the target height that a segment of protective structure would need to protect between those two elevation points. The target height is compared with the three structure types and the simplest structure that can meet the target elevation is chosen for that segment (or if the average elevation between the two points is higher than the DWSEL, no structure is needed and a negligible volume placeholder is selected to enable to model to run). The structure model for the chosen structure type is then applied to calculate the material volume profile for the segment, and a graph node is created with the material values (e.g., sand, aggregate, rebar as appropriate for the given structure) estimate for the length of that structure as it connects to the two elevation data points.

The Port Protector model finds the structural alignment path between the start/end polygons that minimizes the volume of construction materials required while enclosing the port polygon within the parametric coastal protection structure design described above, which is sized to assumed flood level calculated for the seaport. The "model path" around each port consists of two distinct paths: an onshore path that follows around the inland side of the port polygon and an offshore path that goes seaward of the port polygon. Irregularities in topography where some ports are open to the ocean on multiple sides led to both paths using the same algorithm and having access to the same structures, giving one aggregate structure length and volume for the port. Between each elevation datapoint is a distinct "segment" of the path. For each segment, the model takes the mean of the two elevations and subtracts this from the DWSEL to get the "structure crest elevation" (SCE) for that segment. It then optimizes across four choices of structure, as follows:

- If SCE <=0, then no structure is selected (natural terrain provides protection to an acceptable elevation)
- if SCE is 0m - 10m, a flood wall (berm) is selected. (i.e. for Providence (RI), 2.2m-12.m existing grade) – Figure C1
- If SCE is 10m - 15m, rubble breakwater is selected, i.e. -3.2m-2.2m. Figure C2
- If SCE is 15m - 60m, a caisson (or deep) breakwater is selected (i.e. for Providence, -48.237m to -3.237m). Figure C3

For those segments where no structure is needed (i.e., the existing elevation is higher than the DWSEL), the "volume of materials" required is zero. However, to prevent the model from having an almost infinite number of "zero volume" choices, we assigned these segments a value of "length of segment/999" in order to constrain the model path length to a minimum. This adds a negligible increase to the total calculated volume.

The materials required to build gates or entrance/exit facilities were an early consideration that were discarded for the model, as the largest gate would still

represent a very small fraction of the material required and would be very unlikely to affect the projected material volumes in a significant way.

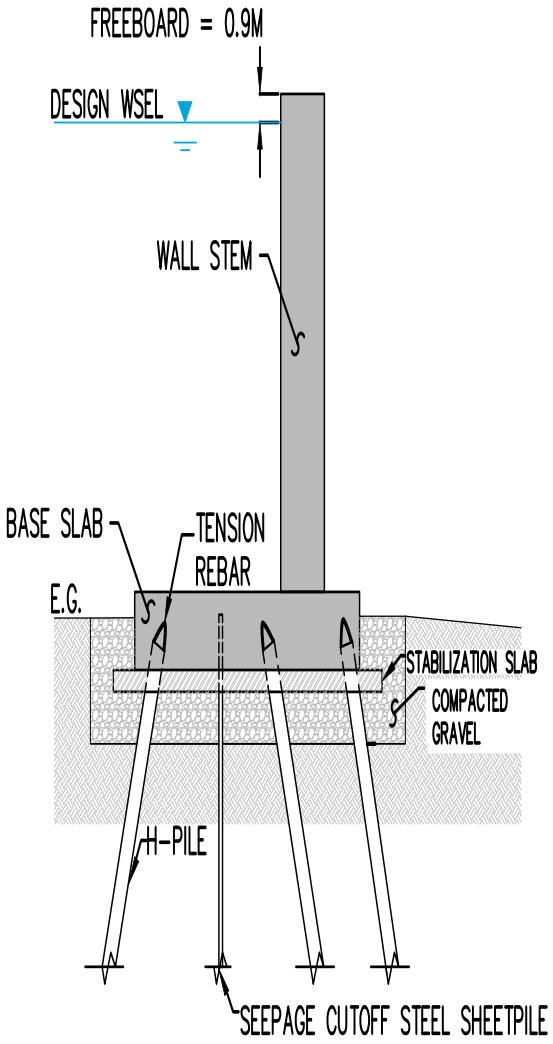

Figure C1 – Floodwall

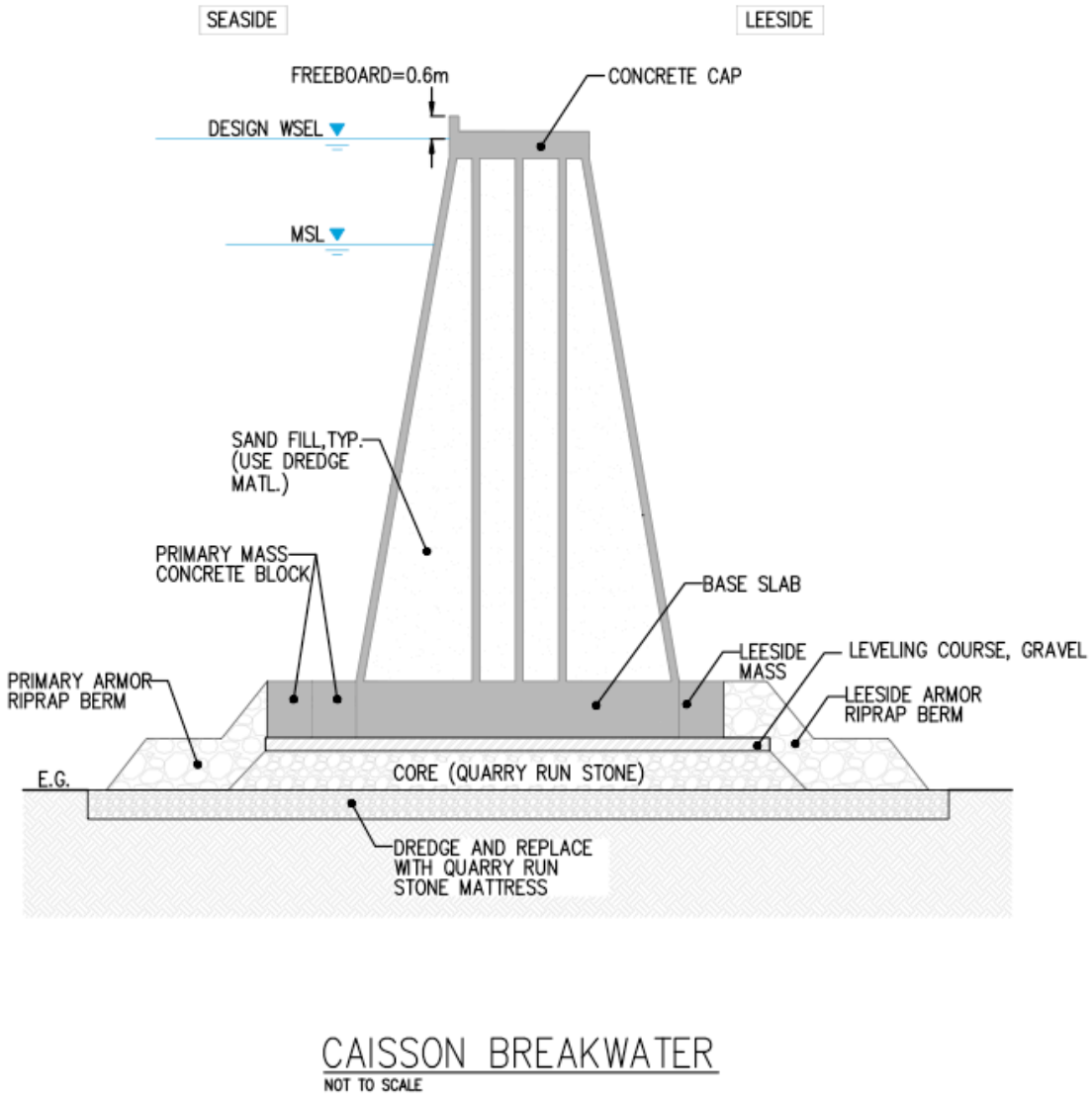

Figure C2 -- Caisson Breakwater

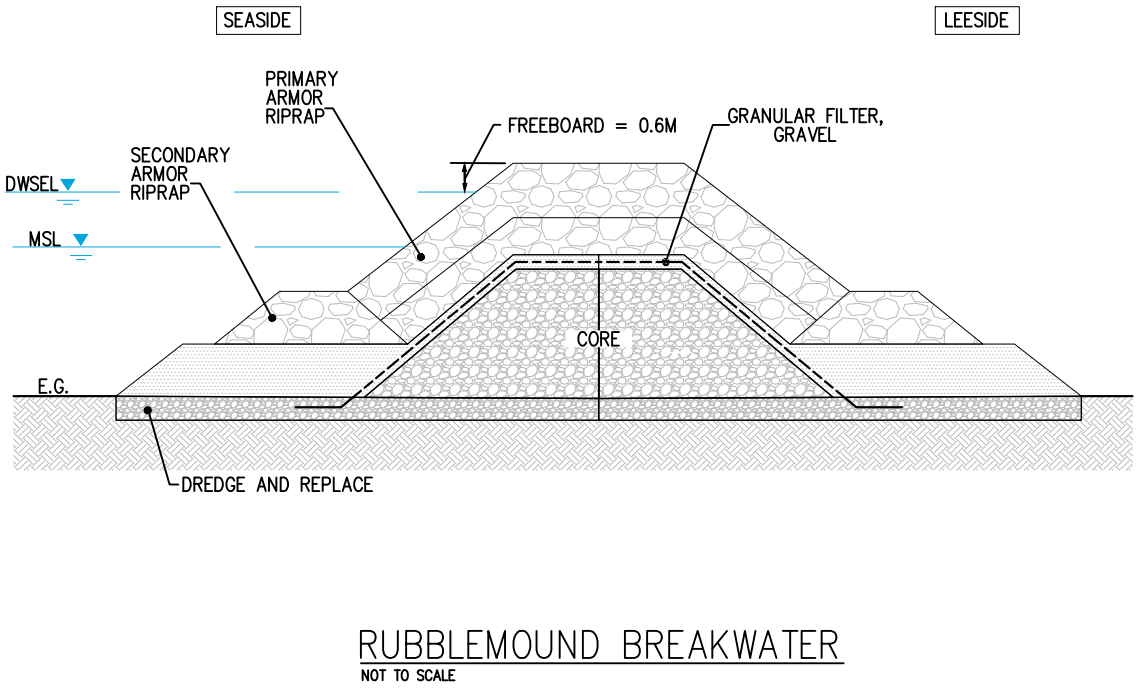

Figure C3 - Rubblemound Breakwater

Example of materials required

As an example of the material profile calculation, the Caisson Breakwater can protect from a DWSEL of at least 15 meters and no more than 60 meters. Three components include the core, the leveling course, and the primary mass. The core is made of quarry run stone, and the volume is height and width multiplied by the segment length. The core height must be at least 2m, but if the DWSEL is greater than 15m, the height is 2 + (DWSEL-25)/3. The core width is a combination of the widths of the cap, the armor, the primary mass, etc. For the leveling course, gravel in required, and the height is always 0.5m, the length is the segment length, and the width is the width of the caisson cap plus the count times width of the primary and leeside mass blocks. The primary mass is concrete block and there are always 2 units. The units are square, and the height/width is the greater of 1.5m or DWSEL/20.

Once the material cost is calculated for every segment according to the model, all of the paths made up of segments that connect the start and end point around the port infrastructure (first in one direction, then in the other) are located, and the minimum cost path for each direction is found using Dijkstra's algorithm. The two paths are combined to find the minimum material volume required for the port

infrastructure to be surrounded at DWSEL. The start/end combined path algorithm is a throwback to an earlier implementation plan that used first one structure around only the seaward side of the port, then two structure types (one 'seaward' and one 'landward' of the port). Several ports with complex topology encouraged the development of three structures considered in a single algorithm, now used in both landward and seaward sides of the port. Future work will update the algorithm to simply encircle the port infrastructure with a single path and not require start/end polygons.

The Port Protector is written in Python and can be accessed through a web interface, though the modeling software runs on a Linux server. The protective structures shown in the paper were chosen based on the required height of protection required. The software converts elevations into material requirements to move through an elevation point, and then builds a weighted graph encompassing all of the possible routes the protective structure could take. Dykstra's algorithm (Dijkstra, 1959) is used to evaluate and compare the possible paths and to choose the lowest material cost path for the protective structure. The output structure from the model has latitude/longitude and elevation information (as well as volumetric material and structure type information) and can be viewed as a port protection structure in Google Earth. Ultimately, we intend the port protector to be publicly available. Thus, users could view information on a port and the modeled protective structure in Google Earth, and even send commands to the server to re-run the simulation with different parameters. All of the elevation datasets are available as well, and the difference in structures based on dataset choice can be seen. Users can even tailor the path and protective structures according to their own preferences. For example, a user could update information regarding the port infrastructure or nuances of the harbor structure by forcing the path to avoid certain areas and protect others (outside of the port polygon that we identified). Additionally, different structure designs could be included in the model to allow for a comparison of materials required by different combinations of designs. A user could also make adjustments for different sea level rise projections, surge height probabilities and tidal ranges. The interface with Google Earth makes the Port Protector user friendly and publicly available. Further development of this aspect is anticipated by the authors.

Appendix D – Method for Converting Concrete to Cement

In order to compare our demand estimates for concrete with the cement capacity estimates discussed in (Fu et al., 2013), we needed a method to convert concrete to cement and standardize the units. For marine concrete calculations, we needed to first convert from cubic yards to cubic meters. We assumed a mix with about 7 sacks of concrete per cy (Concrete Construction 2015), with a sack of cement weighing 94 pounds which resulted in 658 pounds of cement per cy which equals 860 pounds of cement per m3 or 390 kg of cement per m3. We multiplied by 274M m3 of concrete to get 107M t of cement or 16.3% of cement by weight. In many publications we see an assumption of 12.5% of cement by weight for concrete. Using 2,400kg per m3 of concrete, this yields 82.2M t of cement. The difference in ratios is due to the difference in mixes that would be used for 'normal' concrete and marine concrete. The Portland Cement Association's Recommendations for Concrete Mixture Proportioning (PCA 2016), suggest that for corrosion protection for reinforced concrete exposed to deicing salts, brackish water, seawater, or spray from these sources, a maximum water-cement ratio on basis of strength, workability, and finishing needs in 0.4. Depending on the slump wanted, and the maximum aggregate size used, a typical cubic meter of air-entrained concrete could contain anywhere between 267 and 541 kilograms per cubic meter of concrete. A common slump of between 75mm and 100mm and an average large aggregate size of 19mm results in about 345 kilograms of cement per cubic meter of concrete. This applies to most offshore applications and also most structures within a few hundred meters from shore due to the sea spray that could result from storms. For onshore applications, there is a much wider range of water-to-cement ratios that could be assumed. However, in any application for which the concrete should be watertight or exposed to freezing and thawing in a moist condition, which is probably the case in most port applications, the maximum water-to-cement ratio is 0.5. That would result in a cement content of 278 kilograms of cement per cubic meter of concrete.

For more on the maximum water-cement ratios and other numbers, see: (Kosmatka et al., 2011), (USEPA 2015) and (USGS 2006)

Appendix References

AAPA (American Association of Port Authorities), 2011, World Port Rankings 2011, Accessed July 18, 2014, Online at http://aapa.files.cms-plus.com/PDFs/WORLD PORT RANKINGS 2011.pdf.

Concrete Construction (staff), (2015) Concrete in Marine Environments, in: ConcreteConstuction.net (Ed.). http://www.concreteconstruction.net/concrete-articles/concrete-in-marine-environments.aspx

Dijkstra, E.W. (1959) A note on two problems in connexion with graphs. Numerische mathematik, 1, 269-271, ISSN 0029-599X.

Fu, E., Newell, D., Becker, A., Schwegler, B., Fischer, M. (2013) Is Adaptation Sustainable? A Method to Estimate Climate-Critical Construction Resource Capacity. Construction Innovation: Information, Process, Management, 13, 202-216, ISSN 1471-4175.

Hinkel, J., Vuuren, D.P., Nicholls, R.J., Klein, R.J.T. (2012) The effects of adaptation and mitigation on coastal flood impacts during the 21st century. An application of the DIVA and IMAGE models. Climatic Change, 117, 783-794,DOI 10.1007/s10584-012-0564-8, ISSN 0165-0009
1573-1480.

Kosmatka, S.H., Kerkhoff, B., Panarese, W.C. (2011) Design and Control of Concrete Mixtures. Portland Cement Association, ISSN 0893122726.

Muis, S., Verlaan, M., Winsemius, H.C., Aerts, J.C., Ward, P.J. (2016) A global reanalysis of storm surges and extreme sea levels. Nat Commun, 7, 11969,DOI 10.1038/ncomms11969, ISSN 2041-1723 (Electronic)
2041-1723 (Linking), Online at http://www.ncbi.nlm.nih.gov/pubmed/27346549.

NGIA (National Geospatial-Intelligence Agency), (2014) World Port Index, 23rd Edition, Springfield, Virginia, USA. http://msi.nga.mil/MSISiteContent/StaticFiles/NAV_PUBS/WPI/Pub150bk.pdf

Nordpil, 2009, World database of large urban areas, 1950-2050, Accessed July 15, 2014, Online at http://nordpil.com/go/resources/world-database-of-large-cities/.

PCA (Portland Cement Association), (2016) How Concrete is Made. http://www.cement.org/cement-concrete-basics/how-concrete-is-made

USEPA (United States Environmental Protection Agency), (2015) Documentation for Greenhouse Gas Emission and Energy Factors Used in the Waste Reduction Model (WARM). Prepared by ICF International
For the U.S. Environmental Protection Agency
Office of Resource Conservation and Recovery

https://www3.epa.gov/warm/pdfs/WARM_Documentation.pdf

USGS (United States Geological Survey), 2004, Shuttle Radar Topography Mission, 30 Arc Second scenes.

USGS (United States Geological Survey) (2006) Materials in Use in U.S. Interstate Highways. Online at http://pubs.usgs.gov/fs/2006/3127/2006-3127.pdf.

Vafeidis, A.T., Nicholls, R.J., McFadden, L., Tol, R.S.J., Hinkel, J., Spencer, T., Grashoff, P.S., Boot, G., Klein, R.J.T. (2008) A New Global Coastal Database for Impact and Vulnerability Analysis to Sea-Level Rise. Journal of Coastal Research, 244, 917-924,DOI 10.2112/06-0725.1, ISSN 0749-0208
1551-5036.